JOURNAL OF PROPULSION AND POWER
Vol. 25, No. 1, January–February 2009

Chemical Erosion of Refractory-Metal Nozzle Inserts in Solid-Propellant Rocket Motors

Piyush Thakre* and Vigor Yang†
Pennsylvania State University,
University Park, Pennsylvania 16802

DOI: 10.2514/1.37922

An integrated theoretical/numerical framework is established and validated to study the chemical erosion of refractory-metal (tungsten, rhenium, and molybdenum) nozzle inserts in solid-rocket-motor environments, with a primary focus on tungsten. The formulation takes into account multicomponent thermofluid dynamics in the gas phase, heterogeneous reactions at the surface, energy transport in the solid phase, and nozzle material properties. Typical combustion species of nonmetallized ammonium-perchlorate/hydroxyl-terminated-polybutadiene propellants at practical motor operating conditions are considered. The erosion rates calculated by employing three different sets of chemical kinetics data available in the literature for the tungsten-steam reaction have been compared. The effect of considering either of two different tungsten oxides, WO_2 or WO_3, as the final product of surface reactions is also investigated. The predicted erosion rates compare well with experimental data. The oxidizing species of H_2O proved more detrimental than CO_2 in dictating the tungsten nozzle erosion. The material recession rate is controlled by heterogeneous chemical kinetics because the diffusion limit is not reached. The erosion rate increases with increasing chamber pressure, mainly due to higher convective heat transfer and enhanced heterogeneous surface reactions. The tungsten nozzle erodes much more slowly than graphite, but at a rate comparable with that of rhenium. The molybdenum nozzle exhibits the least erosion for flame temperatures lower than 2860 K. Its low melting temperature (2896 K), however, restricts applications for propellants with high flame temperatures.

Nomenclature

A_i = preexponential factor for the rate constant in reaction i
D_{im} = molecular mass diffusivity
E_i = activation energy for reaction i
G = Gibbs free energy
h, H = enthalpy
k = turbulent kinetic energy
$\dot{m}$ = mass flow rate
N = total species numbers
p = pressure
p_t = chamber pressure
Re = Reynolds number
R_u = universal gas constant
$\dot{r}_c$ = net surface recession rate, m/s
$\dot{r}_{i,\mathrm{ch}}$ = chemical-kinetics-controlled recession rate due to species i, $\mathrm{kg/m^2 \cdot s}$
$\dot{r}_{i,\mathrm{diff\text{-}lim}}$ = diffusion-controlled recession rate due to species i, $\mathrm{kg/m^2 \cdot s}$
$\dot{r}_{i,\mathrm{erosion}}$ = recession rate due to species i, $\mathrm{kg/m^2 \cdot s}$
T = temperature
T_t = chamber temperature
U_k = mass diffusion velocity of species k
u, v, w = x, y, and z components of velocity
W_k = molecular weight of species k
W_{mix} = average molecular weight of the gases
W_r = molecular weight of refractory metal
$\dot{w}$ = species molar production rate
Y_k = mass fraction of species k
α = thermal diffusivity
ΔG_R = change in Gibbs free energy
ΔH_R = heat of reaction
Δh_f° = heat of formation (at 298.15 K)
ε = dissipation rate
λ = thermal conductivity
ρ = density
$\dot{\omega}$ = species mass production rate
$\omega_{i,\mathrm{diff\text{-}lim}}$ = maximum diffusion rate of species i toward the surface, $\mathrm{kg/m^2 \cdot s}$

Subscripts

amb = ambient conditions
c = solid phase (refractory metal)
c–g = gas–solid interface
g = gas phase
o = outer boundary of nozzle material
s = surface

I. Introduction

THE erosion of rocket-nozzle materials during motor firings continues to be one of the major hindrances in the advancement of solid-rocket propulsion. A noneroding nozzle is desired, as it maintains a constant nozzle expansion ratio and optimal thrust performance. Graphite and carbon–carbon composites, which have been widely used as nozzle materials, may undergo significant erosion at high chamber pressures and surface temperatures [1,2]. Because a throat-area increase of more than 5% is considered excessive for most solid-rocket applications [3], graphite erosion levels for ultrahigh pressures and long-duration firings can become unacceptable. Different types of erosion-resistant nozzle materials are thus required to further the development of rocket technology. In terms of high melting temperature, refractory metals such as tungsten (W at 3695 K), rhenium (Re at 3459 K), tantalum (Ta at 3290 K),

---

Presented as Paper 1030 at the 46th Aerospace Sciences Meeting of AIAA, Reno, NV, 7–11 January 2008; received 6 April 2008; revision received 24 August 2008; accepted for publication 5 September 2008.

*Ph.D. Candidate, Department of Mechanical and Nuclear Engineering; pkt109@psu.edu. Member AIAA.

†John L. and Genevieve H. McCain Chair in Engineering, Department of Mechanical and Nuclear Engineering; vigor@psu.edu. Fellow AIAA.

molybdenum (Mo at 2896 K), and niobium (Nb at 2750 K) are very attractive. The flame temperatures for aluminized ammonium-perchlorate/hydroxyl-terminated-polybutadiene (AP/HTPB) propellants may reach 3700 K, making tungsten and rhenium promising candidates. One needs to consider, however, not only the melting points of these pure metals, but also their oxides, carbides, and nitrides, because such compounds/eutectics can be formed at the nozzle surface and may modify the chemical behavior of the nozzle material. In general, tungsten nitrides are unstable and dissociate below 1100 K [4]. Consequently, oxidation is likely to dominate, with nitrogen serving as a diluent.

Refractory metals (W, Mo, and Re) and their alloys and carbides [e.g., zirconium carbide (ZrC), tantalum carbide (TaC), and hafnium carbide (HfC)] have exhibited a potential to provide zero-erosion performance [5,6], due to their resistance to chemical attack at high temperatures. The material and processing costs associated with these metals, however, are relatively high. In addition, the high material density increases the inert mass of the vehicle. Metal carbides even suffer from poor thermal shock resistance, leading to the formation of cracks [5,7]. Refractory metals may also form interstitial solutions with the interdiffusion of O, N, or C, which will make the materials more brittle and susceptible to cracking and spalling.

A fundamental understanding of the physiochemical processes dictating the erosion of nozzle material is critical to the development of new materials that can resist erosion more effectively. Experimental data with different materials are scarce, not only because of the high costs involved in conducting measurements at practical rocket-motor conditions, but also because of the proprietary nature of the data. Only a limited amount of information is available in the open literature [5,7,8]. Olcott and Batchelor [5] studied tungsten nozzle inserts and attributed the two principal failure mechanisms to the chemical attack of the propellant combustion gases, H_2O and CO_2, and cracking due to thermal stresses. Results from their subscale motor firings indicated a higher level of erosion with propellants possessing a higher oxidation potential. The addition of 2% thorium dioxide (ThO_2) helped reduce the erosion rate. Arc-cast tungsten with coarse grain was found to be more resistant to the thermal-stress induced fracture than fine-grain tungsten.

Johnston et al. [7] experimentally investigated the performance of a variety of rocket-nozzle materials, including refractory metals (W and Mo), metal carbides (ZrC, TaC, and HfC), graphite, and fiber-reinforced plastics. Three different propellants with flame temperatures of 2865, 3365, and 3810 K were used. Some of the metal-carbide nozzles showed outstanding erosion resistance, comparable with that of the best refractory-metal nozzles. However, all of the metal-carbide nozzles cracked as a result of thermal stresses. Haugen[‡] [8] tested different nozzle materials (including W, Mo, Mo/Re, and W coated with Re) with nonmetallized AP/HTPB propellants.

The overall nozzle erosion process is extremely complex, comprising the interplay of numerous factors, including propellant composition, motor operating conditions, nozzle geometry and material properties, transport of reacting species, and chemical reactions in the gas phase and at the nozzle surface. In addition to chemical erosion, there may also be erosion due to mechanical processes associated with the impingement of metal-oxide particles (e.g., $Al_2O_{3(l)}$) onto the nozzle surface. It is imperative to develop a comprehensive model to accurately explore the erosion process under various rocket-motor operating conditions and to identify materials with effective resistance to erosion. Although a few models [9–12] have been established for treating graphite nozzle erosion, until now there have been few efforts to develop such models for refractory metals. This paper presents the first comprehensive analysis for studying the chemical erosion of refractory-metal nozzle inserts under a broad range of practical rocket-motor environments. Various key mechanisms dictating the nozzle erosion rate for AP/HTPB composite propellants are identified and quantified.

II. Theoretical Formulation

The present work follows the general approach detailed in [12] for graphite erosion and incorporates the physiochemical properties of refractory metals in the combustion streams of AP/HTPB propellants. The formulation involves general conservation equations for the gas phase, energy transport in the solid phase, interfacial conditions between the gas and solid phases, and the outer boundary condition of the nozzle material. The gas-phase dynamics are modeled using the Favre-averaged conservation equations of mass, momentum, energy, and species concentration in axisymmetric coordinates. Turbulence closure is achieved by means of a well-calibrated two-layer turbulence model suitable for transpiration and accelerating flows [12–14]. Full account is taken of variable transport and thermodynamic properties [12].

The current work aims to study the erosion of three refractory metals (W, Re, and Mo), with a primary focus on tungsten. Most existing studies [7,8] have concluded that chemical erosion is the principal cause for the surface recession in nonmetallized propellant environments. In the case of aluminized propellants, mechanical erosion caused by the impingement of metal-oxide particles could also be significant. In addition, there is the possibility of thermite reactions between unoxidized aluminum and metal oxides (e.g., $2Al + WO_3 \rightarrow Al_2O_3 + W$ or $2Al + MoO_3 \rightarrow Al_2O_3 + Mo$) [15]. Such highly exothermic reactions may increase the temperature to a level sufficient to melt the metal nozzle surface [16]. The wetting of metal surfaces by $Al_2O_{3(l)}$ droplets, on the other hand, provides a liquid coating that may help resist further oxidation and erosion. The deposition of $Al_2O_{3(l)}$ may also increase the heat-transfer rate to the nozzle wall. All of the phenomena related to aluminized propellants are still relatively poorly understood and require further investigation. To avoid such complications, only chemical erosion associated with nonmetallized AP/HTPB solid propellants is considered. At sufficiently high temperatures, the metal surface is prone to chemical attack by such oxidizing species as H_2O, CO_2, O_2, and O. Although the reactivity of metals with oxygen is significant [17,18], this effect can be ignored due to the fuel-rich nature of AP/HTPB propellants, which produce negligible amounts of O_2 and O in the gas phase. The main species considered in the combustion stream are thus H_2O, CO_2, CO, HCl, N_2, and H_2. Minor species with negligible concentrations (such as NO, OH, H, O_2 and O) are ignored. The present study further neglects changes in the physiochemical properties of nozzle materials and variations of their melting temperatures due to the possibility of the formation of any eutectics.

A. Heterogeneous Kinetics of Tungsten

Tungsten (W) material is prone to chemical attack by the oxidizing species of H_2O and CO_2 present in the combustion stream of AP/HTPB solid propellant. The effect of HCl is negligible, according to the experimental study by Farber [19]. Chemical-equilibrium calculations [20] also suggest that HCl, H_2, N_2, and CO do not react with W, whereas H_2O and CO_2 show significant reactions. Olcott and Batchelor [5], however, observed that the presence of H_2 and CO, respectively, reduces the reaction rates of H_2O and CO_2 with W. A similar reduction of CO_2 reaction with W due to the presence of CO was observed by Walsh et al. [21].

Several experimental studies have been devoted to the oxidation of tungsten with steam [5,22–26] and CO_2 [5,21] at high temperatures. There seems to be a fair bit of disagreement about the form of the final oxidation product. Some consider [5,23] $WO_{3(g)}$ as the major oxidation product, whereas others [21,27] have suggested $WO_{2(g)}$ as the major product. Greene and Finfork [25] found that the oxide formed has a stoichiometry of $WO_{2.7}$, which indicates that both WO_3 and WO_2 may be present. Kalipatrick and Lott [24] performed experiments over a temperature range of 1273–1973 K to determine the mechanism of the tungsten reaction with steam at atmospheric pressure. The measured activation energies were 48.9 and 22.7 kcal/mol in the temperature ranges of 1273–1723 and 1723–1973 K, respectively. At temperatures greater than 1723 K, it was suggested that the final oxidation products could be either the vapor

---

[‡] Private communication with S. Haugen, 2007.

phase WO_3 and its polymers or the volatile $WO_3 \cdot H_2O_{(g)}$. The rate-determining step was proposed to be the oxidation of $WO_{2(s)}$ to $WO_3 \cdot H_2O_{(g)}$ and $WO_{3(g)}$ and its polymers. Based on the observations of Belton and McCarron [26], the major species could be $WO_3 \cdot H_2O_{(g)}$, which is formed due to the reaction of WO_3 and H_2O in the gas phase. Such a reaction, if it occurs, could be effective at reducing the amount of H_2O attacking the surface and hence the erosion rate. The chemical-equilibrium calculations [20] also show that $WO_{3(l,g)}$ and its polymers are the major products at high temperature, as described in Table 1. For temperatures above 1700 K, a thermodynamic analysis based on Gibbs free energy indicates that formation of $WO_{3(g)}$ is favored (Appendix A). In the current study, both $WO_{3(g)}$ and $WO_{2(g)}$ are considered individually as the final oxidation product. The chemical pathways and kinetics data are summarized in Table 2. The decrease in the reaction rate of CO_2 and W due the presence of CO is accounted as a function of the ratio of the mole fractions of CO and CO_2 [21]. Whenever the reaction order with respect to H_2O is not mentioned explicitly in the literature, a first-order reaction is assumed.

B. Heterogeneous Kinetics of Molybdenum

Although molybdenum (Mo) has performed satisfactorily as a nozzle throat insert and a structural support material, its usefulness is limited by its relatively high ductile-to-brittle transition temperature [3] and low melting point. The use of Mo inserts is usually restricted to propellants with lower flame temperatures. The oxidation of molybdenum at high temperature yields $H_{2(g)}$ and volatile MoO_3 [28,29]. The chemical-equilibrium calculations [20] show that $MoO_{3(g)}$ and its polymers are the major products at high temperatures, as listed in Table 3. Kalipatrick and Lott [29] experimentally investigated the oxidation of Mo under different mass flow rates of steam. In the current study, the kinetics data corresponding to the maximum mass flow rate are adopted, as they represent the condition closest to the kinetically limited reaction rates. Table 2 gives the chemical kinetics data for the oxidation of Mo by steam at high temperatures. First-order kinetics with respect to H_2O are assumed, as it is not explicitly mentioned in [29]. The reaction of CO_2 with Mo is not included in the present work due to the lack of relevant kinetics data in the literature. The thermodynamic analysis based on Gibbs free energy (Appendix A), however, indicates that the reaction of Mo with CO_2 may be as significant as that of W with CO_2.

C. Heterogeneous Kinetics of Rhenium

Rhenium (Re)-based nozzle inserts can be used for propellants with high flame temperatures due to the high melting temperature of rhenium. They are also widely used in small liquid rocket engines [30]. The oxidation of rhenium by steam at high temperatures has been experimentally studied [31,32]. Kalipatrick and Lott [31] suggested that the oxide formed is Re_2O_7, which is volatile at high temperatures. Table 2 lists the chemical kinetics data for the oxidation of Re by steam. Duriez [32] concluded that the reaction is first order with respect to H_2O. The reaction rate was found to be highly dependent on the mass flow rate of the steam and the gas velocity, indicating that the experimental conditions were not close to the kinetically limited case. In the current study, the kinetics data of Kalipatrick and Lott [31] are chosen because the data fit well for all the steam flow rates considered. The reaction of CO_2 with Re is not included, as no kinetics data relevant to this reaction is found in the literature. Unlike the reaction of CO_2 and W, the reaction of CO_2 and Re is not likely to be significant, due to the higher oxidation resistance of Re. No thermodynamic analysis of the oxidation reaction based on Gibbs free energy was performed because of the lack of thermodynamic properties for rhenium oxides.

D. Chemical Reactions at the Nozzle Surface

The rate of consumption of metal by an oxidizing species i is expressed as

$$\dot{r}_{i,\mathrm{ch}} = k_i p_{i,s}^n \ (\mathrm{kg/m^2\,s}) \tag{1}$$

where

$$p_{i,s} = p_s Y_{i,s} \frac{W_{\mathrm{mix},s}}{W_i} \tag{2}$$

$$k_i = A_i \exp(-E_i/R_u T_s) \tag{3}$$

Table 1 Chemical-equilibrium calculations [20] for tungsten oxidation (reactants at 2800 K, 40 atm, and mass ratio of 1:1)

Reactants	H_2O	CO_2	$WO_{3(l)}$	WO_3 and its polymers	H_2	CO	WO_2	ΔH_R, kJ/kg	ΔG_R, kJ/kg
W/H_2O	0.35	——	0.12	0.51	0.02	——	∼0	−2910.20	−23,939.10
W/CO_2	——	0.14	0.42	0.21	——	0.23	∼0	−2285.98	−13,354.6

Table 2 Chemical kinetics data for heterogeneous surface reactions of tungsten

Surface reaction	A_i	E_i, kcal/mol	$\dot{\omega}$, kg/m$^2 \cdot$ s	Temperature range, K	Reference
		Tungsten[a]			
$W + 3H_2O_{(g)} \rightarrow WO_{3(g)} + 3H_{2(g)}$	8.64 kg/m$^2 \cdot$ s $\cdot$ atm	22.70	$k_i p_{H_2O}$	1723–1973	Kalipatrick and Lott [24]
or $W + 2H_2O_{(g)} \rightarrow WO_{2(g)} + 2H_{2(g)}$	5.722×10^4 kg/m$^2 \cdot$ s $\cdot$ atm	48.13	$k_i p_{H_2O}$	1073–1973	Unal et al. [22]
$W + 3CO_{2(g)} \rightarrow WO_{3(g)} + 3CO_{(g)}$	1.433×10^4 kg/m$^2 \cdot$ s $\cdot$ atm	47.23	$k_i p_{H_2O}$	1073–1623	Greene and Finfork [25]
or $W + 2CO_{2(g)} \rightarrow WO_{2(g)} + 2CO_{(g)}$	4.026×10^3	79.00	$k_i p_{CO_2}^{0.88}$	2200–3200	Walsh et al. [21]
		Molybdenum[a]			
$Mo + 3H_2O_{(g)} \rightarrow MoO_{3(g)} + 3H_{2(g)}$	4.48 kg/m$^2 \cdot$ s $\cdot$ atm	57.5	$k_i p_{H_2O}$	1373–1973	Kalipatrick and Lott [29]
		Rhenium[a]			
$2Re + 7H_2O_{(g)} \rightarrow Re_2O_{7(g)} + 7H_{2(g)}$	29.85 kg/m$^2 \cdot$ s $\cdot$ atm	29.80	$k_i p_{H_2O}$	1123–1973	Kalipatrick and Lott [31]
$2Re + 7H_2O_{(g)} \rightarrow Re_2O_{7(g)} + 7H_{2(g)}$	57.97 kg/m$^2 \cdot$ s $\cdot$ atm	34.90	$k_i p_{H_2O}$	1873–2473	Duriez [32]

[a] The rate of consumption is obtained in kg/m^2/s; $k_i = A_i \exp(-E_i/R_u T_s)$.

Table 3 Chemical-equilibrium calculations [20] for molybdenum oxidation (reactants at 2800 K, 40 atm, and mass ratio 1:1)

Reactants	H_2O	CO_2	$Mo_{(c)}$	MoO_3 and its polymers	H_2	CO	ΔH_R, kJ/kg	ΔG_R, kJ/kg
Mo/H_2O	0.36	——	0.26	0.36	0.015	——	−2497.07	−24,292.3
Mo/CO_2	——	0.15	0.25	0.38	——	0.22	−1828.15	−13,692.9

In the preceding equations, $Y_{i,s}$ and $p_{i,s}$ represent the mass fraction and partial pressure of species i at the surface, respectively; $W_{\mathrm{mix},s}$, p_s, and T_s are the molecular weight of the gas mixture, pressure, and temperature at the surface, respectively; and n is the overall order of the heterogeneous reaction. The mass rate of consumption of an oxidizing species i at the gas–solid interface is given by [12]

$$\bar{\dot{\omega}}_i = \dot{r}_{i,\mathrm{ch}} \frac{\nu_i W_i}{\nu_r W_r} \tag{4}$$

where ν_i and ν_r are the stoichiometric coefficients for the particular surface reaction under consideration, as listed in Table 2.

E. Solid-Phase Governing Equation

With the neglect of thermal decomposition and chemical reactions in the solid phase, the heat conduction in the radial direction is governed by the following equation:

$$\rho_c \frac{\partial h_c}{\partial t} + \frac{\rho_c}{r}\frac{\partial}{\partial r}(r h_c \dot{r}_c) = \frac{1}{r}\frac{\partial}{\partial r}\left(\lambda_c r \frac{\partial T_c}{\partial r}\right) \tag{5}$$

The equation takes into account the effect of surface recession and variable thermophysical properties. The integration of Eq. (5) at a steady-state condition across the nozzle material gives

$$r_i\left[\lambda_c \frac{\partial T_c}{\partial r}\right]_{r_i} = \dot{r}_c \rho_c (h_{c-g} r_i - h_o r_o) + r_o\left[\lambda_c \frac{\partial T_c}{\partial r}\right]_{r_o} \tag{6}$$

where r_i and r_o are the inner and outer radii, respectively, of the nozzle material at any axial location, and $c{-}g$ and h_o are the corresponding specific enthalpies.

In most existing studies, the outer boundary of the nozzle material is modeled to be adiabatic. This treatment is valid when the nozzle material is sufficiently thick or well insulated and the thermal conductivity is low. Considering the high thermal conductivity of refractory metals, however, the thermal penetration depth ($\sim\alpha_c/\dot{r}_c$) in the nozzle material under typical motor operating conditions could be of the same order as the thickness of the insert. Thus, the enforcement of the adiabatic condition needs to be carefully examined. An adequate sensitivity study on the effect of the outer boundary condition on the nozzle material erosion is elaborated later.

F. Gas–Solid Interfacial Condition

The processes in the gas and solid phases are matched at the nozzle surface by enforcing the continuities of mass, species, and energy fluxes. This procedure eventually gives the erosion rate of nozzle material and the surface temperature. The conservation laws at the gas–solid interface can be written as follows:

Mass:

$$\bar{\rho}_g \tilde{u}_r = \rho_c \dot{r}_c \tag{7}$$

Species:

$$\left(-\bar{\rho}_g D_{km} \frac{d\tilde{Y}_k}{dr} + \bar{\rho}_g \tilde{Y}_k \tilde{u}_r\right) = \bar{\dot{\omega}}_k \tag{8}$$

Energy:

$$\left[\lambda_c \frac{\partial T_c}{\partial r}\right]_{r_i} + \dot{r}_c \rho_c h_{c-g} = \left[\lambda_g \frac{\partial \tilde{T}_g}{\partial r}\right]_{r_i} + \sum_{k=1}^{N} \bar{\dot{\omega}}_k \tilde{h}_{g,k} \tag{9}$$

where $\tilde{u}_r$ stands for the radial velocity in the gas phase due to material erosion. The rate of production of the gas-phase species k at the nozzle surface on account of heterogeneous reactions is denoted by $\bar{\dot{\omega}}_k$. The first term in Eq. (9) can be obtained by considering the overall energy balance in the solid phase represented by Eq. (6). Radiation is neglected in Eq. (9) due to the prevalence of convective heat transfer in a nonmetallized propellant environment. Flow symmetry is enforced along the nozzle centerline.

G. Nozzle Recession Rate

Owing to heterogeneous surface reactions, species-concentration gradients are formed in the nozzle flowfield and cause the diffusion of those species toward or away from the surface. At a high surface temperature, heterogeneous chemical reactions can proceed so rapidly that the erosion rate could be dictated entirely by species diffusion. The diffusion-controlled recession rate $\dot{r}_{i,\mathrm{diff\text{-}lim}}$ due to a specific oxidizing species i can be determined by first calculating $\bar{\dot{\omega}}_{i,\mathrm{diff\text{-}lim}}$ from Eq. (8) with $\tilde{Y}_i = 0$ and then applying the following equation:

$$\dot{r}_{i,\mathrm{diff\text{-}lim}} = \bar{\dot{\omega}}_{i,\mathrm{diff\text{-}lim}} \frac{\nu_r W_r}{\nu_i W_i} \tag{10}$$

At low surface temperatures, heterogeneous reactions become the rate-controlling process for nozzle erosion, due to reduced chemical activity. The recession rate $(\mathrm{kg/m^2 \cdot s})$ associated with an oxidizing species i is obtained as

$$\dot{r}_{i,\mathrm{erosion}} = \min(\dot{r}_{i,\mathrm{diff\text{-}lim}}, \dot{r}_{i,\mathrm{ch}}) \tag{11}$$

The net recession rate (m/s) of the nozzle surface is determined by

$$\dot{r}_c(x) = \frac{1}{\rho_c}\sum_i \dot{r}_{i,\mathrm{erosion}} \tag{12}$$

III. Numerical Treatment

The governing equations and associated boundary conditions are solved numerically by means of a density-based finite volume approach with body-fitted coordinates. A four-stage Runge–Kutta scheme is used for the time integration. The convective fluxes are treated explicitly with a second-order central-difference scheme, following the methodology proposed by Rai and Chakravarthy [33]. The chemical reaction source terms are handled in a semi-implicit manner. To ensure numerical stability and convergence, a fourth-order artificial dissipation based on the scalar dissipation model by Swanson and Turkel [34] is employed. The code has been implemented on a parallel computing facility by employing a distributed-memory message passing interconnection. The grid is stretched in the radial direction and clustered near the surface. The centers of the computational cells adjacent to the nozzle surface are located at $y^+ < 1$ to accurately capture the near-wall phenomena.

IV. Nozzle Configurations and Boundary Conditions

Figure 1 shows the baseline nozzle configuration considered here. The geometry is identical to that employed in our previous study on graphite material [12] so that a direct comparison of the erosion rates of different materials can be made. The incoming flow consists of the combustion products of nonmetallized AP/HTPB composite propellants. The chamber pressure p_t and temperature T_t are specified at the nozzle inlet. The velocity at the exit is supersonic. Table 4 lists the species mass fractions at the inlet obtained from the chemical-equilibrium calculation [20] at $p_t = 6.9$ MPa. Six different chamber pressures and their corresponding temperatures are used to study the effect of motor operating conditions on nozzle erosion. The species mass fractions remain nearly constant in the pressure range of 6.9–45 MPa. The ambient temperature is taken as 300 K. The thermophysical properties of W, Mo, and Re are adopted as polynomial functions of temperature.

The discussion of results is organized as follows. First, tungsten erosion for the baseline nozzle configuration is studied by employing the different surface chemical kinetic schemes outlined in Sec. II. Based on the results, appropriate kinetics data and reaction products are chosen for further parametric studies. The chemical erosion model is then validated against experimental data for W, Mo, and Re, as summarized in Table 5. The nozzle geometry and inlet flow conditions exactly simulate those in the corresponding experimental studies.

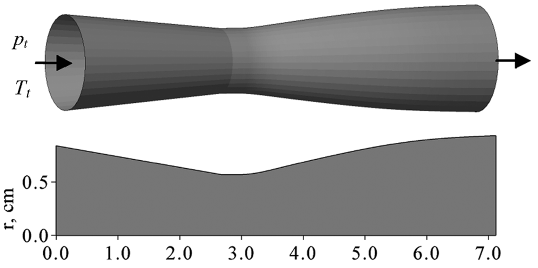

Fig. 1 Baseline nozzle configuration.

V. Results and Discussions

The theoretical/numerical framework described in the preceding sections was implemented to explore the chemical erosion of refractory-metal (W, Mo, and Re) nozzles in practical rocket-motor environments. The axisymmetric computational domain of the rocket nozzle, shown in Fig. 1, is divided into 141 × 80 grid points in the x and r directions. The turbulent flow development in the same nozzle configuration was detailed earlier [12]. To simulate the erosion of the tungsten nozzle, two heterogeneous reactions of W with H_2O and CO_2, along with the energy balance given by Eq. (9), are implemented at the surface. The oxidizing species CO_2 and H_2O are consumed to form CO, H_2, and gaseous tungsten oxides (WO_3 or WO_2). Concentration gradients are then established near the wall. The gas-phase reactions among the AP/HTPB combustion-product species were not included because of their negligible effect on nozzle erosion [12]. It should be noted that for tungsten and other refractory metals, volatile oxides (e.g., WO_3 and WO_2) formed at the nozzle surface may react with $HCl_{(g)}$ to generate compounds such as $WO_2Cl_{2(g)}$. Such gas-phase reactions do not have any significant impact on the nozzle erosion rate, as they will not affect either the concentrations of H_2O and CO_2 species or the rate of heat transfer to the nozzle wall.

As shown in Table 2, three different sets of kinetics data [22,24,25] are available for the reaction between W and H_2O at high temperatures. It is important to make a judicious selection of the data that yield the most accurate erosion rate. Figure 2 shows a comparison of the predicted tungsten nozzle erosion rates based on different chemical kinetics data. The incoming flow temperature and pressure are $T_t = 3000$ K and $p_t = 6.9$ MPa, respectively, and the outer boundary of the nozzle material is assumed to be adiabatic. The maximum erosion rates obtained from the three sets of kinetics data [22,24,25] are 0.078, 0.069, and 0.047 mm/s, respectively. The most severe erosion occurs near the throat, due to the enhanced heat transfer in that region. The measured erosion rates of tungsten nozzle inserts obtained from various experimental studies[§] [7,8] with similar nozzle throat diameters consistently lie in the range of 0.02–0.05 mm/s. On this basis, the kinetics data of Kalipatrick and Lott [24], which lead to the lowest erosion rate, appear to be most appropriate for the present application. The small wiggle in the erosion-rate profile arises from the discontinuity in the slope of nozzle contour at the entrance of the throat region. Such small irregularities were not observed in other cases with smooth-nozzle profiles shown later.

The stoichiometry of surface reactions and the overall heat of reaction depend strongly on the final product species, which in turn affect the calculated surface temperature and erosion rate. Existing experimental studies on tungsten oxidation [5,21,23,27] have suggested either $WO_{2(g)}$ or $WO_{3(g)}$ as the final oxidation product. To clarify the effect of this choice on the predicted erosion rates, calculations were performed for both $WO_{2(g)}$ or $WO_{3(g)}$. Figure 3 shows a comparison of the predicted tungsten nozzle erosion rates obtained by considering either $WO_{3(g)}$ ($\Delta h_f^o = -319.725$ kJ/mol) or $WO_{2(g)}$ ($\Delta h_f^o = 29.062$ kJ/mol) as the final oxidation product of surface reactions. The chemical kinetics data from Kalipatrick and Lott [24] are used. The use of $WO_{3(g)}$ gives rise to an erosion rate that is 0.005 mm/s lower. It is possible that if the oxidation product emerging from the surface is WO_2, then it may further react with H_2O to form either $WO_{3(g)}$ or $WO_2(OH)_{2(g)}$ [24]. This process reduces the oxidation potential of combustion products by depleting the concentration of H_2O, thereby causing a reduced erosion rate. A similar situation occurs if the oxidation product $WO_{3(g)}$ reacts with water to form $WO_2(OH)_{2(g)}$. Although such reactions can take place in the gas phase, the lack of associated kinetics data renders their inclusion in the analysis futile. In the present study, all the further

Table 4 Nozzle inlet flow conditions[a]

Combustion-product species (nonmetallized AP/HTPB)	
Y_{H_2O}	0.29
Y_{CO_2}	0.22
Y_{CO}	0.11
Y_{H_2}	0.01
Y_{N_2}	0.10
Y_{HCL}	0.27
Motor operating conditions	
p_t, MPa	6.9, 10, 15, 25, 35, 45
T_t, K	3000, 3020, 3040, 3050, 3060, 3065
T_{amb}, K	300

[a] Tungsten density is 19.25 g/cm^3, throat radius is 0.57 cm, and average thickness is 4.8 cm.

Table 5 Experimental studies of refractory-metal nozzle erosion

Reference	Nozzle material
Johnston et al. [7]	W, Mo, refractory compounds
Haugen [8]	Mo, W, Mo/Re, W/Re

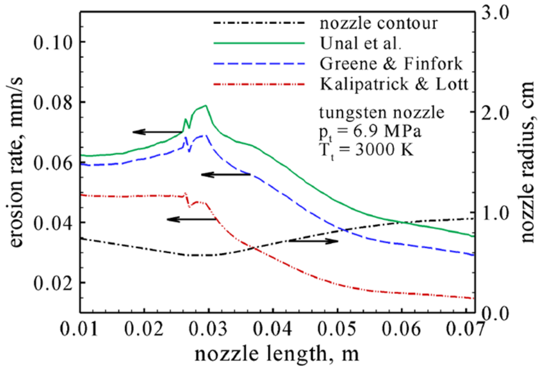

Fig. 2 Tungsten nozzle erosion rate with different chemical kinetics (Unal et al. [22], Kalipatrick and Lott [24], and Greene and Finfork [25]) using $WO_{3(g)}$ as the final oxidation product.

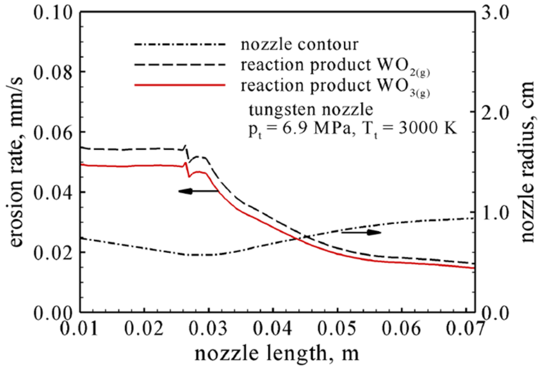

Fig. 3 Tungsten nozzle erosion rate using different final oxidation products and chemical kinetics from Kalipatrick and Lott [24].

[§] Private communication with S. Haugen, 2007.

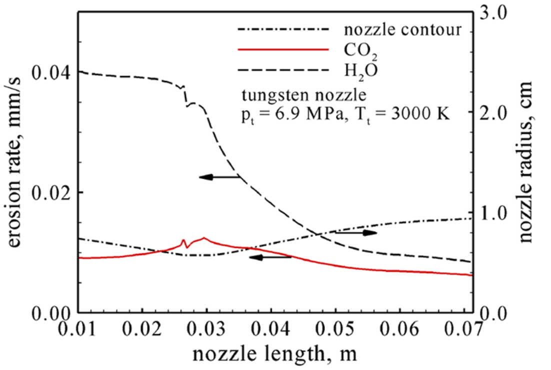

Fig. 4 Tungsten nozzle erosion rate due to individual oxidizing species H_2O and CO_2.

calculations for tungsten nozzles are performed by considering the kinetics data of Kalipatrick and Lott [24] with the following surface reactions:

Reaction R1:

$$W + 3H_2O \rightarrow WO_3 + 3H_2$$

Reaction R2:

$$W + 3CO_2 \rightarrow WO_3 + 3CO$$

Figure 4 shows the nozzle erosion rates caused by each of the oxidizing species, H_2O and CO_2. The former proves to be much more detrimental (about 3 times) than the latter, a situation similar to graphite nozzle erosion [12].

The dependence of the erosion rate on the outer boundary condition of the nozzle material was examined, because this condition affects the nozzle surface temperature and associated chemical reaction rates. Table 6 lists three different outer boundary conditions considered herein. The baseline adiabatic condition was relaxed by allowing convective heat transfer at the outer boundary. The outer heat-transfer coefficient h_{amb}, estimated from standard correlations for turbulent flows over a flat plate, falls in the range of 100–500 $\mathrm{W/m^2 \cdot K}$, depending on the specific configuration of the nozzle assembly and vehicle speed. Figure 5 shows that the calculated erosion rate decreases slightly with enhanced heat transfer at the outer boundary, due to the decrease in the nozzle inner surface temperature. The erosion rate calculated by employing the adiabatic outer nozzle boundary thus represents the upper limit. Table 6 summarizes the results. All the calculations presented subsequently are based on the adiabatic outer boundary of the nozzle material unless mentioned otherwise.

Figure 6 shows the entire nozzle flowfield in terms of the temperature, Mach number, and mass fractions of H_2O, CO_2, CO, and H_2. The Mach number increases from 0.28 at the inlet to 2.3 at the exit, but the temperature decreases monotonically from a value slightly less than that of the chamber condition to about 1900 K. The endothermic surface reactions and conductive heat transfer through the nozzle material help lower the surface temperature. The thickness of the species-concentration boundary layer (δ_c) is greater than its velocity counterpart and can be estimated using a simple order-of-magnitude analysis as follows:

$$\delta_c \sim \sqrt{D_{\mathrm{eff}} \tau_f} \tag{13}$$

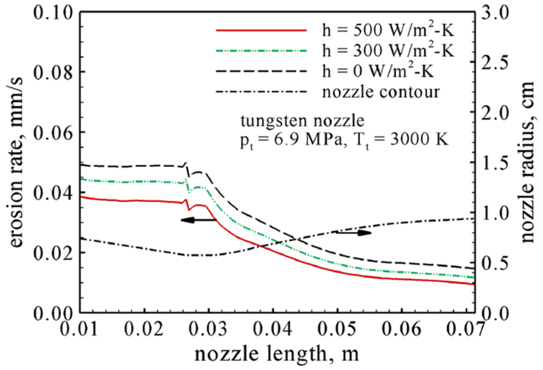

Fig. 5 Effect of nozzle outer boundary condition on erosion rate.

where D_{eff} is the effective mass diffusivity on the order of $10^{-2}\ \mathrm{m^2/s}$. The flow residence time τ_f is approximated as the ratio of the nozzle length to the average axial velocity and has a value of about 0.1 ms. Based on Eq. (13), the concentration boundary-layer thickness is about 1 mm, which is close to that observed in Fig. 6.

At a quasi-steady-state condition, whether the species diffuse toward or away from the surface depends on the sign of the species gradient dY_k/dr at the surface, as governed by the following equation, which is a rearranged form of Eq. (8):

$$\left(\frac{d\tilde{Y}_k}{dr}\right) = \frac{(-\bar{\dot{\omega}}_k + \bar{\rho}_g \tilde{Y}_k \tilde{u}_r)}{\bar{\rho}_g D_{km}} \tag{14}$$

The species gradient in turn depends on two factors: the rate of production/consumption of species $\dot{\omega}_k$ and surface blowing velocity u_r. Because H_2O and CO_2 are consumed at the surface (i.e., negative $\dot{\omega}_k$), their gradients are always positive, with diffusion toward the surface. The direction of CO and H_2 diffusion, however, is affected by the relative magnitudes of $\dot{\omega}_k$ and u_r. As a result of the dominance of reaction R1 in dictating the erosion rate, a large amount of H_2 is produced and diffuses away from the surface. In the case of graphite nozzle erosion [12], because both the surface reactions of $C_{(s)}$ with H_2O and CO_2 yield CO, the higher value of $\dot{\omega}_{CO}$ dominates the effect of u_r. Consequently, the mass fraction of CO at the surface becomes much higher than that in the core flow, causing it to diffuse away from the surface throughout the nozzle length. For a tungsten nozzle, however, only a limited amount of CO emerges from the surface through reaction R2, leading to a low value of $\dot{\omega}_{CO}$. In the upstream converging section of the nozzle, as a consequence of high surface blowing (higher erosion rate), the mass fraction of CO is lower than in the core flow and CO diffuses toward the surface. In the downstream region, however, the low surface blowing (lower erosion rate) reverses the situation. Figure 7 clearly shows the distributions of mass fraction of CO and temperature at the nozzle surface.

Figure 8 compares tungsten and graphite nozzle erosion rates for the same operating condition and nozzle configuration. The erosion rate at the graphite nozzle throat (0.124 mm/s) is about 2.6 times that of tungsten (0.047 mm/s). This suggests that tungsten (19.25 $\mathrm{g/cm^3}$), which is approximately 10 times denser than graphite (1.9 $\mathrm{g/cm^3}$), actually exhibits a higher mass consumption rate ($\mathrm{g/cm^2 \cdot s}$). The lower erosion rate of tungsten is thus attributed to its higher density. It is clear from Eq. (12) that the net nozzle erosion rate is inversely proportional to its material density.

Table 6 Effect of outer boundary condition of nozzle on the tungsten erosion rate[a]

Outer boundary condition $[\partial T_c/\partial r]_{r_o} = h_{\mathrm{amb}}(T_{c,o} - T_{\mathrm{amb}})$	Erosion rate at throat, mm/s	Inner surface temperature at the throat, K
Adiabatic	0.047	2450
$h_{\mathrm{amb}} = 300\ \mathrm{W/m^2}$, $T_{c,o} = 600$ K	0.042	2390
$h_{\mathrm{amb}} = 500\ \mathrm{W/m^2}$, $T_{c,o} = 600$ K	0.036	2320

[a] $T_{\mathrm{amb}} = 300$ K, $T_t = 3000$ K, and $p_t = 6.9$ MPa.

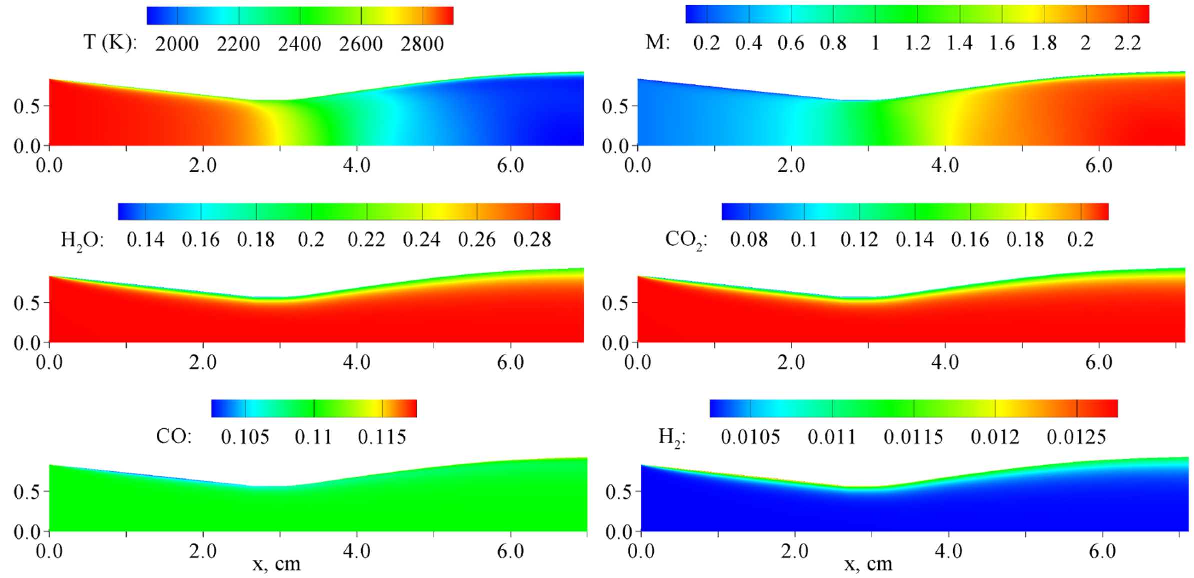

Fig. 6 Distributions of temperature, Mach number and mass fractions of H_2O, CO_2, CO, and H_2 in the nozzle ($T_t = 3000$ K and $p_t = 6.9$ MPa, with surface reactions and conductive wall).

The radial distributions of temperature and oxidizing-species concentrations are instrumental in identifying the mechanisms of nozzle material erosion. Figures 9 and 10 show the radial distributions of temperature at the throat and at a downstream location, respectively. The temperature at the throat decreases monotonically from 2785 K at the centerline to 2450 K at the surface. The corresponding values at the downstream location are 2280 and 2550 K, respectively, but the radial profile does not decrease monotonically. The temperature rise near the surface results from the dissipation of the flow kinetic energy into thermal energy. The lower surface temperature at the throat, as compared with its counterpart at the downstream location, is attributed to the higher rate of endothermic heterogeneous reactions at the throat. Figures 11 show the radial distributions of species mass fractions at the nozzle throat. The finite concentrations of H_2O and CO_2 at the surface indicate that erosion is kinetically controlled.

The effect of chamber pressure on nozzle erosion rate was also studied. Figure 12 shows the distribution along the entire length of the tungsten nozzle at various chamber pressures. The maximum value is attained in the throat region for all cases. It is worth noting

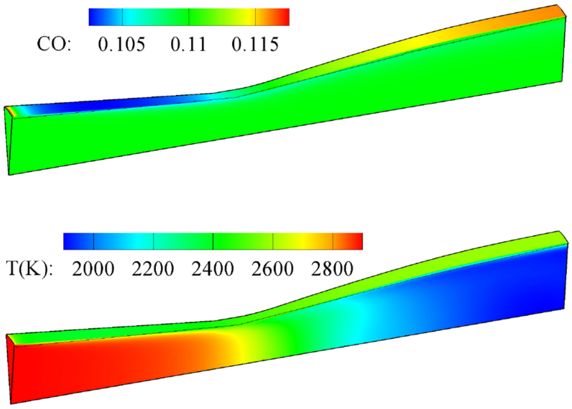

Fig. 7 A tilted view of the nozzle showing distributions of temperature and mass fractions of CO ($T_t = 3000$ K and $p_t = 6.9$ MPa, with surface reactions and conductive wall).

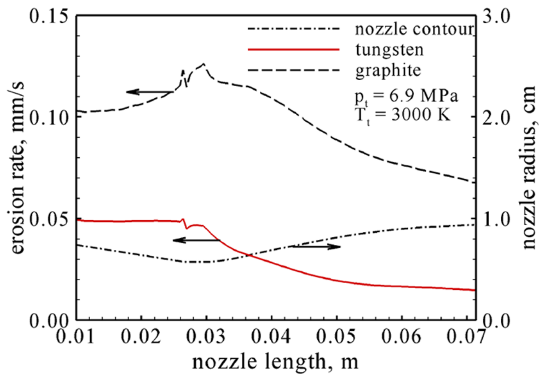

Fig. 8 Comparison of erosion rates of graphite and tungsten nozzles.

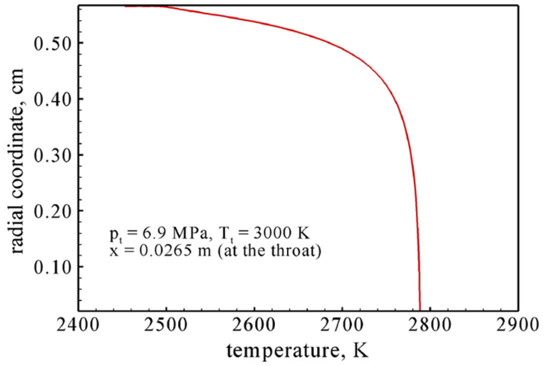

Fig. 9 Radial distribution of temperature at the tungsten nozzle throat.

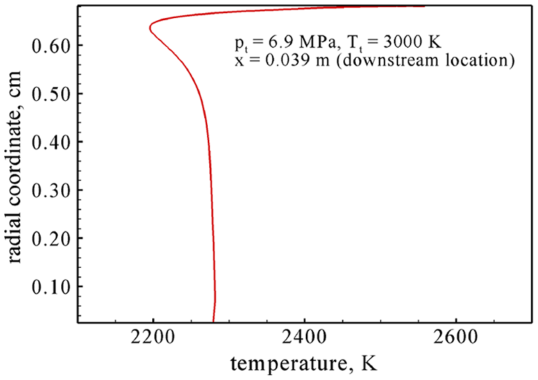

Fig. 10 Radial distribution of temperature at a location downstream of the nozzle throat.

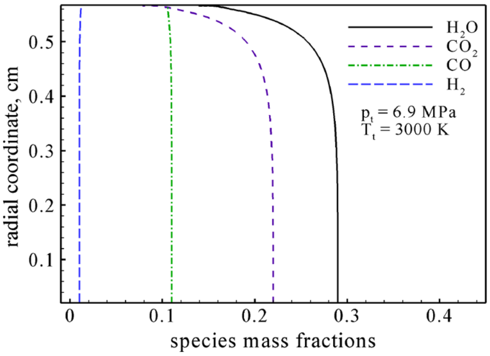

Fig. 11 Radial distributions of species concentrations at the nozzle throat.

from Fig. 2 that for surface reactions with lower activation energies, the peak in the erosion-rate profile spreads more widely in the upstream region than the cases with higher activation energies. As the pressure increases, the peak becomes more prominent at the throat, as evidenced in Fig. 12. The surface temperature, pressure, and activation energies of surface reactions are thus the three factors most instrumental in determining the characteristics of the erosion-rate profile. Figure 13 shows the linear variations of the tungsten and rhenium erosion rates at the throat with the chamber pressure. Because the convective heat-transfer rate increases with pressure, there is a corresponding rise in the erosion rate. The lower value of the rhenium erosion rate, as compared with that of tungsten, can be attributed to the lack of including CO_2 reaction in the former case. The observations based solely on the effect of the H_2O reaction show that the erosion rates of tungsten and rhenium are comparable, especially taking into account the scatter in the kinetics data from the experimental studies.

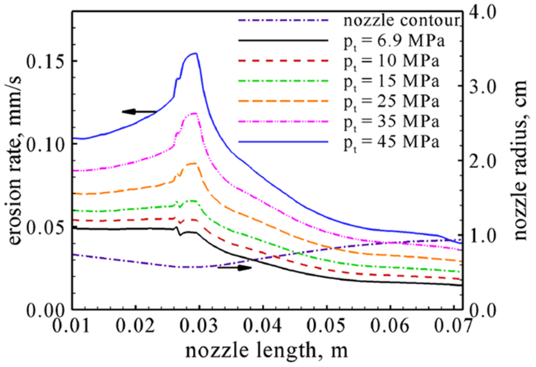

Fig. 12 Distributions of tungsten erosion rates along the nozzle length at various chamber pressures.

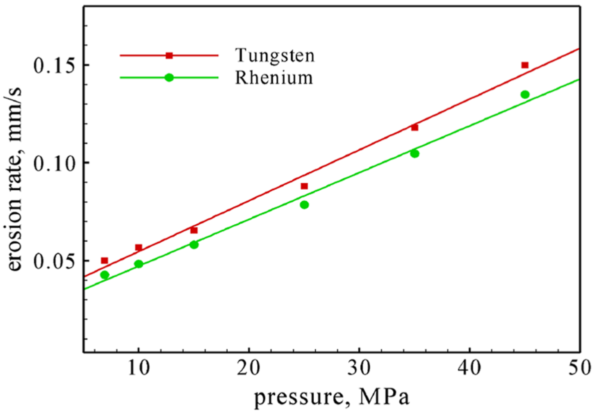

Fig. 13 Effect of chamber pressure on tungsten and rhenium erosion rates at the nozzle throat.

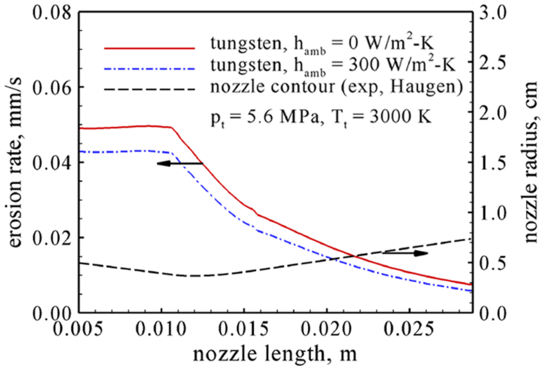

Fig. 14 Calculated tungsten nozzle erosion rate for the experimental study by Haugen (private communication with S. Haugen, 2007).

To validate the current analysis, calculations were performed to simulate the nozzle-erosion experiments by Johnston et al. [7] and Haugen [8]. The nozzle geometries and inlet flow conditions exactly simulate those in the corresponding experimental studies. Table 7 summarizes the inlet conditions in terms of mass fractions of the species and motor operating conditions. Haugen reported the tungsten nozzle recession data from an earlier subscale motor firing of the Penguin Mk3 missile. The erosion rate was deduced from measurements of the thrust and chamber pressure over the firing duration. The nozzle material was tungsten with 2% La_2O_3, and the propellant used was nonmetallized AP/HTPB (88:11) with 1% additives. The nozzle surface showed some deposition of silica released from the upstream thermal insulation. Figure 14 shows the calculated nozzle erosion rate along with the nozzle contour for the inlet conditions listed in Table 7. The erosion-rate profile peaks in the nozzle throat region. Because the nozzle contour is very smooth, the erosion profile does not exhibit any irregularity, unlike the situation with the nozzle contour in Fig. 2. The calculated erosion rate of 0.047 mm/s closely matches the measured value of 0.040 mm/s. The slight overprediction may be attributed to two facts: the assumption of an adiabatic outer boundary and the neglect of gas-phase reactions of tungsten oxide with H_2O. Silica deposition, detected in the postfiring analysis, may also contribute to the decrease in the measured throat diameter. If heat transfer is allowed at the outer boundary, the predicted erosion rate is lowered marginally to 0.042 mm/s, as shown in Fig. 14. The uncertainty of the kinetics data employed for heterogeneous reactions also affects the calculated erosion rate.

The second validation was performed based on the extensive experimental work of Johnston et al. [7] to evaluate the performance of several rocket-nozzle materials, including W, Mo, refractory-metal carbides, and graphite. The instantaneous throat radius was obtained from measurements of the thrust and chamber pressure, as well as postfiring analyses. The high-density tungsten nozzles performed well with only slight-to-moderate erosion. One of the propellants used was Arcite 368 (polyvinyl chloride and ammonium perchlorate). The inlet conditions based on this nonmetallized propellant are summarized in Table 7. Although the arc-cast tungsten nozzle obtained from the commercial supplier showed an erosion rate of 0.028 mm/s, the molybdenum nozzle insert did not erode at

Table 7 Inlet conditions for simulations of experiments

Reference	Y_{CO_2}	Y_{H_2O}	Y_{H_2}	Y_{CO}	Y_{HCL}	Y_{N_2}	p_t, MPa	T_t, K
Haugen[a b]	0.21	0.28	0.01	0.10	0.29	0.11	5.6	3000
Johnston [c][7]	0.20	0.27	0.01	0.12	0.30	0.10	6.9	2860
Haugen [d][8]	0.16	0.26	0.01	0.20	0.27	0.10	6.9	2810

[a] Private communication with S. Haugen, 2007.

[b] Tungsten density is 19.25 g/cm^3, throat radius is 0.4 cm, and average thickness is 3 cm.

[c] Tungsten density is 19.25 g/cm^3, molybdenum density is 21.20 g/cm^3, throat radius is 0.39 cm, and average thickness is 1 cm.

[d] Tungsten density is 19.25 g/cm^3, rhenium density is 21.20 g/cm^3, throat radius is 0.53 cm, and average thickness is 2 cm.

Table 8 Comparison between calculated and measured nozzle erosion rates

Reference (propellant)	Nozzle material	$\dot{r}_{\mathrm{expt}}$, mm/s	$\dot{r}_{\mathrm{model}}$, mm/s
Haugen[a] (AP/HTPB)	W with 2% La_2O_3	0.040	0.047 (adiabatic outer boundary) 0.042 ($h_{\mathrm{amb}} = 300\ \mathrm{W/m^2 \cdot K}$)
Johnston et al.[7] (Arcite 368)	Arc-cast W	0.028	0.041 (adiabatic outer boundary) 0.037 ($h_{\mathrm{amb}} = 500\ \mathrm{W/m^2 \cdot K}$)
	Molybdenum	Negligible	Negligible
Haugen [8] (AP/HTPB)	W with 2% La_2O_3	0.020–0.030	0.040 (adiabatic outer boundary) 0.035($h_{\mathrm{amb}} = 500\ \mathrm{W/m^2 \cdot K}$)
	Recoated W	Not mentioned	0.032 (adiabatic outer boundary)

[a] Private communication with S. Haugen, 2007.

all. Figure 15 shows calculated erosion-rate profiles for the tungsten and molybdenum nozzle inserts, along with the nozzle contour. The maximum convective heat-transfer and erosion rates occurred slightly upstream of the throat. For a curved nozzle with a large angle of convergence, the wall heat transfer usually reaches its maximum just before the throat. Such a phenomenon has been observed both experimentally [35] as well as computationally [11] for curved nozzles. The calculated erosion rate with an adiabatic outer nozzle boundary is 0.041 mm/s for tungsten and nearly zero for molybdenum, as shown in Fig. 15. If this adiabatic condition is relaxed, then the predicted erosion rate decreases. The measured erosion rate could, in fact, be lower due to the fact that gas-phase reactions between volatile tungsten oxides and H_2O may reduce the oxidation potential of the propellant.

The third validation study was based on experiments by Haugen [8]. The nozzle materials tested on the subscale motor were W, Mo, Mo/Re, and W coated with Re. A reduced-smoke AP/HTPB propellant was employed with varying compositions. Table 7 summarizes the nozzle geometry and inlet conditions. The validity of erosion-rate measurements remains to be clarified [8], as heavy silica deposition from the upstream region protected the nozzle surface from exposure to the combustion species for a major part of the firing duration. The erosion rate for the tungsten nozzle was reported to be in the range of 0.02–0.03 mm/s, whereas the values for other materials were not mentioned. It was concluded, however, that the best insert material was rhenium-coated tungsten. The molybdenum insert showed negligible erosion, with the propellant having a lower flame temperature (2476 K), but the erosion increased drastically at a higher flame temperature (2810 K). This is in contrast to the negligible erosion for the Mo insert observed by Johnston et al. [7] for a similar flame temperature (2860 K). Figure 16 shows the calculated erosion rates for tungsten and rhenium, along with the nozzle contour. The erosion rates at the nozzle throat are 0.040 and 0.032 mm/s for W and Re, respectively. Table 8 summarizes the comparison of all the calculated and measured erosion rates at the throat. The slight discrepancies may be attributed to the uncertainties of the chemical kinetics data for surface reactions and the adiabatic outer boundary condition employed.

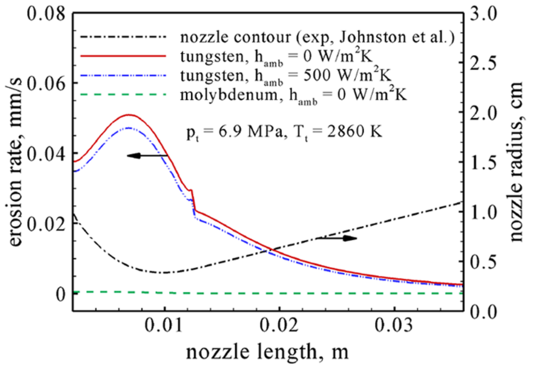

Fig. 15 Calculated tungsten and molybdenum nozzle erosion rate for the experimental study by Johnston et al. [7].

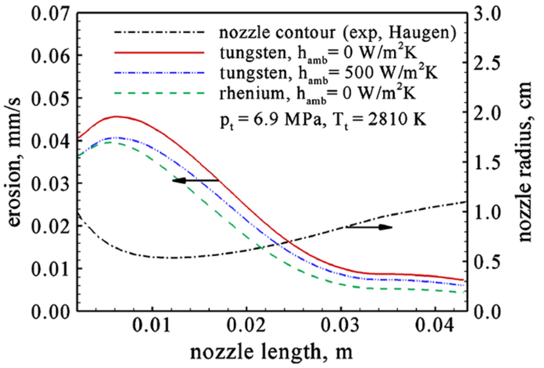

Fig. 16 Calculated tungsten and rhenium nozzle erosion rate for the experimental study by Haugen [8].

VI. Conclusions

A comprehensive analysis has been established to predict the chemical erosion of refractory-metal (tungsten, molybdenum, and rhenium) nozzle materials in rocket motors with nonmetallized AP/HTPB solid propellants. The primary focus was on the tungsten nozzle. The predicted erosion rates matched reasonably well with three different sets of measurements. H_2O proved to be the more detrimental oxidizing species than CO_2 in dictating tungsten nozzle erosion. The material recession rate is controlled by heterogeneous chemical kinetics and increases linearly with the chamber pressure. To improve the model predictivity, more accurate chemical properties for heterogeneous reactions of refractory metals with oxidizing species at realistic rocket-motor operating conditions are needed. The gas-phase kinetics of volatile tungsten oxides and steam also needs to be studied further and incorporated into the analysis to account for the fact that a reduction in H_2O concentration may reduce the erosion rate. The erosion rate for tungsten was found to be much lower than for graphite, but comparable with that of rhenium. The least erosion was exhibited by molybdenum, for which the implementation, however, is restricted to propellants with lower flame temperatures (less than 3000 K) due to its low melting point.

Appendix A: Thermodynamic Analysis of Surface Chemical Reactions

The spontaneity and favorability of a chemical reaction depend on the change in Gibbs free energy associated with the reaction. Gibbs free energy is defined as follows:

$$G = H - TS \tag{A1}$$

The change in Gibbs free energy at a constant temperature and pressure is given by

$$\Delta G = \Delta H - T\Delta S \tag{A2}$$

A chemical reaction is spontaneous if $\Delta G < 0$. Equation (A2) indicates that even for endothermic reactions ($\Delta H < 0$), a situation similar to the present surface reactions, the process can be spontaneous if $\Delta G < 0$: that is, if $T\Delta S > \Delta H$. Clearly, high temperature favors the progress of an endothermic reaction. In addition, the more negative the value of ΔG, the more favorable the reaction becomes.

When chemical kinetics data for a given surface reaction are not available, the related change in Gibbs free energy can help identify whether the reaction will take place. It can further assist in the

Table A1 Changes in Gibbs free energies for different surface reactions

Reaction	T, K	ΔH_R, kJ	ΔS_R, J/K	$\Delta G_R = \Delta H_R - T\Delta S_R$, kJ
$W + 3CO_{2(g)} \rightarrow WO_{3(g)} + 3CO_{(g)}$	2800	498.250	180.866	−17.174
$W + 2CO_{2(g)} \rightarrow WO_{2(g)} + 2CO_{(g)}$	2800	564.023	184.158	48.380
$Mo + 3CO_{2(g)} \rightarrow MoO_{3(g)} + 3CO_{(g)}$	2800	435.629	174.674	−52.425

characterization of final oxidation products when there is an uncertainty and/or difference of opinion associated with it. Table A1 lists Gibbs free energies for different surface reactions at 1 atm and 2800 K. The latter is typical of the nozzle surface temperature in a rocket-motor environment. Because the pressure dependence of surface reactions is not known to be significant, the analysis should be reasonably valid at higher pressures. All the thermodynamic properties are from McBride et al. [36]. No calculation for the rhenium-oxidation reaction was performed due to the lack of thermodynamic data for rhenium oxides. In the case of tungsten oxidation when different final products are considered, the change in Gibbs free energy is negative for $WO_{3(g)}$ but positive for $WO_{2(g)}$, indicating the spontaneity and prevalence of the former product. The change in Gibbs free energy of Mo oxidation by CO_2 has a more negative value than its counterpart for W. The former reaction is thus spontaneous and likely to occur at 2800 K.

Acknowledgments

This work was supported by the U.S. Office of Naval Research as a part of Multi-University Research Initiative (MURI) project funded under contract N00014-04-1-0683, with Judah Goldwasser and Cliff Bedford as contract monitors. The authors are deeply grateful to Steinar Haugen of Nammo Raufoss AS, Norway, Richard Yetter, and Justin Sabourin for experimental data and technical advice.

References

[1] Geisler, R. L., "The Relationship Between Solid-Propellant Formulation Variables and Nozzle Recession Rates," JANNAF Rocket Nozzle Technology Subcommittee Meeting, Lancaster, CA, July 1978.

[2] Swope, L. W., and Berard, M. F., "Effects of Solid-Rocket Propellant Formulations and Exhaust-Gas Chemistries on the Erosion of Graphite Nozzles," AIAA Solid Propellant Rocket Conference, Palo Alto, CA, Jan. 1964.

[3] Wong, E. Y., "Solid Rocket Nozzle Design Summary," 4th AIAA Propulsion Joint Specialist Conference, Cleveland, OH, AIAA Paper 68-665, 1968.

[4] Toth, L., *Transition Metal Carbides and Nitrides*, Academic Press, New York, 1971.

[5] Olcott, E. L., and Batchelor, J. D., "Failure Mechanisms in Dense Tungsten Alloy Rocket Nozzles," *Journal of Spacecraft and Rockets*, Vol. 1, No. 6, 1964, pp. 635–642.
doi:10.2514/3.27714

[6] Opeka, M. M., Talmy, I. G., Wuchina, E. J., Zaykoski, J. A., and Causey, S. J., "Mechanical, Thermal, and Oxidation Properties of Refractory Hafnium and Zirconium Compounds," *Journal of the European Ceramic Society*, Vol. 19, Nos. 13–14, 1999, pp. 2405–2414.
doi:10.1016/S0955-2219(99)00129-6

[7] Johnston, J. R., Signorelli, R. A., and Freche, J. C., "Performance of Rocket Nozzle Materials with Several Solid Propellants," NASA TN D-3428, 1966.

[8] Haugen, S., "Noneroding Nozzle Throat Material for Rocket Motors with AP-Based Propellant," 34th AIAA/ASME/SAE/ASEE Joint Propulsion Conference, AIAA Paper 98-3972, July 1998.

[9] Delaney, L. J., Eagleton, L. C., and Jones, W. H., "A Semiquantitative Prediction of the Erosion of Graphite Nozzle Inserts," *AIAA Journal*, Vol. 2, No. 8, 1964, pp. 1428–1433.
doi:10.2514/3.2570

[10] Acharya, R., and Kuo, K. K., "Effect of Pressure and Propellant Composition on Graphite Rocket Nozzle Erosion Rate," *Journal of Propulsion and Power*, Vol. 23, No. 6, 2007, pp. 1242–1254.
doi:10.2514/1.24011

[11] Shimada, T., Sekiguchi, M., and Sekino, N., "Flow Inside a Solid Rocket Motor with Relation to Nozzle Inlet Ablation," *AIAA Journal*, Vol. 45, No. 6, 2007, pp. 1324–1332.
doi:10.2514/1.22952

[12] Thakre, P., and Yang, V., "Chemical Erosion of carbon–carbon/Graphite Nozzles in Solid-Propellant Rocket Motors," *Journal of Propulsion and Power*, Vol. 24, No. 4, 2008, pp. 822–833.
doi:10.2514/1.34946

[13] Rodi, W., "Experience with Two-Layer Models Combining the k-e Model with a One-Equation Model Near the Wall," 29th Aerospace Sciences Meeting, Reno, NV, AIAA Paper 1991-0216, 1991.

[14] Tseng, I. S., and Yang, V., "Combustion of a Double-Base Homogeneous Propellant in a Rocket Motor," *Combustion and Flame*, Vol. 96, No. 4, 1994, pp. 325–342.
doi:10.1016/0010-2180(94)90102-3

[15] Sanders, V. E., Asay, B. W., Foley, T. J., Tappan, B. C., and Pacheco, A. N., "Reaction Propagation of Four Nanoscale Energetic Composites (Al/MoO_3, Al/WO_3, Al/CuO, and Bi_2O_3)," *Journal of Propulsion and Power*, Vol. 23, No. 4, 2007, pp. 707–714.
doi:10.2514/1.26089

[16] Wang, L. L., Munir, Z. A., and Maximov, Y. M., "Thermite Reactions: Their Utilization in the Synthesis and Processing of Materials," *Journal of Materials Science*, Vol. 28, No. 14, 1993, pp. 3693–3708.
doi:10.1007/BF00353167

[17] Walsh, P. N., Quets, J. M., and Graff, R. A., "Kinetics of the Oxygen-Tungsten Reaction at High Temperatures," *Journal of Chemical Physics*, Vol. 46, No. 3, 1967, pp. 1144–1153.
doi:10.1063/1.1840781

[18] Gulbransen, E. A., Andrew, K. F., and Brassart, F. A., "Kinetics of Oxidation of Pure Tungsten, 1150°C to 1615°C," *Journal of the Electrochemical Society*, Vol. 111, No. 1, 1964, pp. 103–109.
doi:10.1149/1.2426043

[19] Farber, M., "High-Temperature Reaction Rates of Several Metals with Hydrogen Chloride and Water Vapor," *Journal of the Electrochemical Society*, Vol. 106, No. 9, 1959, pp. 751–754.
doi:10.1149/1.2427491

[20] Gordon, S., and McBride, B. J., "Computer Program for Calculation of Complex Chemical Equilibrium Compositions and Applications," NASA Rept. 1311, 1994.

[21] Walsh, P. N., Quets, J. M., Graff, R. A., and Ladd, I. R., "Kinetics of the Oxidation of Tungsten by CO_2 at High Temperatures," *Journal of Chemical Physics*, Vol. 46, No. 9, 1967, pp. 3571–3576.
doi:10.1063/1.1841259

[22] Unal, C., Bohl, W. R., and Pasamehmetoglu, K. O., "Modeling of Heat and Mass Transfer in Accelerator Targets during Postulated Accidents," *Nuclear Engineering and Design*, Vol. 196, No. 2, 2000, pp. 185–200.
doi:10.1016/S0029-5493(99)00297-6

[23] Smolik, G. R., McCarthy, K. A., Petti, D. A., and Coates, K., "Hydrogen Generation from Steam Reaction with Tungsten," *Journal of Nuclear Materials*, Vols. 258–263, No. 2, 1998, pp. 1979–1984.
doi:10.1016/S0022-3115(98)00169-X

[24] Kalipatrick, M., and Lott, S. K., "Reaction of Flowing Steam with Refractory Metals 3: Tungsten," *Journal of the Electrochemical Society*, Vol. 113, No. 1, 1966, pp. 17–18.
doi:10.1149/1.2423850

[25] Greene, G. A., and Finfork, C. C., "Vaporization of Tungsten in Flowing Steam at High Temperatures," *Experimental Thermal and Fluid Science*, Vol. 25, No. 3, 2001, pp. 87–99.
doi:10.1016/S0894-1777(01)00063-2

[26] Belton, G. R., and McCarron, R. L., "The Volatilization of Tungsten in the Presence of Water Vapor," *Journal of Physical Chemistry*, Vol. 68, No. 7, 1964, pp. 1852–1856.
doi:10.1021/j100789a030

[27] Harvey, F. J., "High Temperature Oxidation of Tungsten Wires in Water Vapor-Argon Mixtures," *Metallurgical Transactions*, Vol. 5, No. 5, 1974, pp. 1189–1192.
doi:10.1007/BF02644332

[28] Gulbransen, E. A., Andrew, K. F., and Brassart, F. A., "Oxidation of Molybdenum, 550°C to 1700°C," *Journal of the Electrochemical Society*, Vol. 110, No. 9, 1963, pp. 952–959.
doi:10.1149/1.2425918

[29] Kalipatrick, M., and Lott, S. K., "Reaction of Flowing Steam with

Refractory Metals 1: Molybdenum (1100–1700°C)," *Journal of Physical Chemistry*, Vol. 69, No. 5, 1965, pp. 1638–1640. doi:10.1021/j100889a032

[30] Schoenman, L., "4000 of Materials for Low-Thrust Rocket Engines," *Journal of Propulsion and Power*, Vol. 11, No. 6, 1995, pp. 1261–1267. doi:10.2514/3.23967

[31] Kalipatrick, M., and Lott, S. K., "Reaction of Flowing Steam with Refractory Metals 2: Rhenium (850–1700°C)," *Journal of the Electrochemical Society*, Vol. 113, No. 1, 1966, pp. 15–16. doi:10.1149/1.2423848

[32] Duriez, C., "Rhenium Oxidation by Steam at High Temperatures," *Oxidation of Metals*, Vol. 61, Nos. 1–2, 2004, pp. 49–67. doi:10.1023/B:OXID.0000016276.26446.34

[33] Rai, M. M., and Chakravarthy, S., "Conservative High-Order Accurate Finite Difference Method for Curvilinear Grids," AIAA Paper 93-3380, 1993.

[34] Swanson, R. C., and Turkel, E., "On Central-Difference and Upwind Schemes," *Journal of Computational Physics*, Vol. 101, No. 2, 1992, pp. 292–306. doi:10.1016/0021-9991(92)90007-L

[35] Back, L. H., Massier, P. F., and Gier, H. L., "Convective Heat Transfer in a Convergent-Divergent Nozzle," *International Journal of Heat and Mass Transfer*, Vol. 7, No. 5, 1964, pp. 549–568. doi:10.1016/0017-9310(64)90052-3

[36] McBride, B. J., Zehe, M. J., and Gordon, S., "NASA Glenn Coefficients for Calculating Thermodynamic Properties of Individual Species," NASA TP-2002-211556, 2002.

S. Son
Associate Editor